directly perpendicular to the axis of compression (*28*). This is in agreement with our prediction. In the gold nanoparticle layers shown in Fig. 1C, wrinkles are more easily seen because of the strong scattering of the metal cores. As the image shows, the length scale over which the fold forms (*l*) is set by the initial wrinkle wavelength (λ).

Understanding compaction of nanometer-thin membranes through controllable and reversible modes like wrinkling and folding opens the door to technological use of these systems (*29*). In medicine, developing synthetic lung surfactant formulations depends on our capability to reproduce the incredible ability of native lung surfactant to compact by folding (*9*). Likewise, nanoparticle thin film applications rely on understanding the mechanical properties and responses of such layers (*12*, *13*, *29*). From wrinkle wavelengths, constants like the bending modulus can be found (*5*, *6*, *30*), whereas controlling the wrinkle-to-fold transition can help the development of adaptive functions in new technologies like flexible electronics (*29*, *31*).

References and Notes

1. T. A. Witten, *Rev. Mod. Phys.* **79**, 643 (2007).
2. A. Lobkovsky, S. Gentges, H. Li, D. Morse, T. A. Witten, *Science* **270**, 1482 (1995).
3. D. Vella, P. Aussillous, L. Mahadevan, *Europhys. Lett.* **68**, 212 (2004).
4. L. Bourdieu, J. Daillant, D. Chatenay, A. Braslau, D. Colson, *Phys. Rev. Lett.* **72**, 1502 (1994).
5. J. Huang *et al.*, *Science* **317**, 650 (2007).
6. N. Bowden, S. Brittain, A. G. Evans, J. W. Hutchinson, G. M. Whitesides, *Nature* **393**, 146 (1998).
7. R. Huang, Z. Suo, *J. Appl. Phys.* **91**, 1135 (2002).
8. H. Diamant, T. A. Witten, C. Ege, A. Gopal, K. Y. C. Lee, *Phys. Rev. E* **63**, 061602 (2001).
9. J. A. Zasadzinski, J. Ding, H. E. Warriner, F. Bringezu, A. J. Waring, *Curr. Opin. Colloid Interface Sci.* **6**, 506 (2001).
10. A. Gopal, K. Y. C. Lee, *J. Phys. Chem. B* **105**, 10348 (2001).
11. C. P. Collier, T. Vossmeyer, J. R. Heath, *Annu. Rev. Phys. Chem.* **49**, 371 (1998).
12. D. G. Schultz *et al.*, *J. Phys. Chem. B* **110**, 24522 (2006).
13. K. E. Mueggenburg, X. M. Lin, R. H. Goldsmith, H. M. Jaeger, *Nat. Mater.* **6**, 656 (2007).
14. S. T. Milner, J. F. Joanny, P. Pincus, *Europhys. Lett.* **9**, 495 (1989).
15. A. Saint-Jalmes, F. Graner, F. Gallet, B. Houchmandzadeh, *Europhys. Lett.* **28**, 565 (1994).
16. Q. Zhang, T. A. Witten, *Phys. Rev. E* **76**, 041608 (2007).
17. E. S. Nikomarov, *Langmuir* **6**, 410 (1990).
18. W. Lu *et al.*, *Phys. Rev. Lett.* **89**, 146107 (2002).
19. E. Cerda, L. Mahadevan, *Phys. Rev. Lett.* **90**, 074302 (2003).
20. Supporting material is available on *Science* Online.
21. H. Hertz, *Wiedemann's Ann. Phys. Chem. (Kyoto)* **22**, 449 (1884).
22. Although both up and down folds are observed, we note that the down fold is favored over the up fold. This asymmetry is not present in the numerics and can be accounted for by considering the meniscus geometry at the polyester/water/air contact line. Given that the wetting angle at the contact line is constant, the meniscus on the up fold will be slightly larger than the down fold. This geometric difference generates a slight asymmetry in the gravitational energy for the two states and favors the down fold. However, our current work has been done in a "deep" water regime. The up fold is more likely to be observed when the subphase is very shallow because the down fold cannot develop.
23. In certain conditions, a stretched state could play the role of a wrinkled state. The specific energy (U/L) for both has a finite value independent of system size. On the other hand, the specific energy of a folded state for a given applied strain Δ/L diverges to negative values for large systems. This predicts that a direct transition from a stretched to a folded state could be possible for large systems. The external compression necessary to observe a transition from a stretched flat surface to a wrinkled state is $\Delta_0 = L \times 2(BK)^{1/2}/Et$, where t is film thickness. The critical compression for the wrinkle to fold transition is $\Delta_1 = \lambda/3$. So a wrinkled state should be observed before folding if the inequality $\Delta_0 < \Delta_1$ or $L/\lambda < [3/(8\pi^2)](\lambda/t)^2$ is satisfied.
24. K. Efimenko *et al.*, *Nat. Mater.* **4**, 293 (2005).
25. H. E. Ries, W. A. Kimball, *J. Phys. Chem.* **59**, 94 (1955).
26. C. Ybert, W. Lu, G. Moller, C. M. Knobler, *J. Phys. Condens. Matter* **14**, 4753 (2002).
27. Solid monolayers continue to have positive surface tensions measured by Wilhelmy plates when they fold (*8*, *10*). Whereas the Wilhelmy plate accurately measures all interfacial forces at liquid interfaces, the measurement breaks down when the interface becomes solidlike (*32*). For a solid monolayer capable of supporting a deviatoric shear stress, a small increase in pressure at the periphery should lead to a smaller increase at the plate, with the weakening being governed by the ratio of shear to bulk moduli of the monolayer. Thus, parts of the monolayer close to the barriers may be under a compressive stress even if a finite surface tension is measured at the plate.
28. A. Gopal, V. A. Belyi, H. Diamant, T. A. Witten, K. Y. C. Lee, *J. Phys. Chem. B* **110**, 10220 (2006).
29. R. Vaia, J. Baur, *Science* **319**, 420 (2008).
30. The wrinkle wavelength observed in our experiments gives $B \sim 15$ kT for the gold layer. Using $B = Eh^3/12(1 - \nu^2)$, where t is the film thickness and ν is its Poisson ratio, we estimate the Young's modulus (E) of the 15-nm gold trilayer with $\nu = 0.3$ on the order of 100 kPa.
31. D.-H. Kim *et al.*, *Science* **320**, 507 (2008); published online 25 March 2008, 10.1126/science.1154367.
32. A. Saint-Jalmes, M. Assenheimer, F. Gallet, *J. Phys. Chem. B* **102**, 5810 (1998).

33. We thank T. Witten for many fruitful discussions as well as his leadership of the NSF Inter-American Materials Collaboration: Chicago-Chile (DMR-0303072) under whose support this collaboration began; M. Meron for many rich discussions; S. Rice, F. Melo, J. Pavez, A. Pocivavsek, and K. Lam for experimental help; and E. Sultan and A. Boudaoud for sharing their unpublished/in press manuscript "The Buckling of a Swollen Thin Gel Layer Bound to a Compliant Substrate" with us for guidance. This work was supported in part by the University of Chicago Materials Research Science and Engineering Center program of the NSF (DMR-0213745) and the U.S.-Israel Binational Foundation (2006076). L.P. thanks the University of Chicago Medical Scientist Training Program for support; A.K. was supported by the Dreyfus Summer Research Program at the University of Chicago (SG-06-039); K.Y.C.L. is grateful for support from March of Dimes (No. 6-FY07-357); R.D. and B.L. acknowledge the support of NSF/U.S. Department of Energy grant no. CHE-0535644 for ChemMatCARS; and E.C. acknowledges the support of Anillo Act 15, Fondap grant no. 11980002 and Fondecyt Project no. 1050083.

Supporting Online Material

www.sciencemag.org/cgi/content/full/320/5878/912/DC1
Materials and Methods
SOM Text
Fig. S1
Movies S1 and S2

12 December 2007; accepted 14 April 2008
10.1126/science.1154069

Metasomatized Lithosphere and the Origin of Alkaline Lavas

Sébastien Pilet,* Michael B. Baker, Edward M. Stolper

Recycled oceanic crust, with or without sediment, is often invoked as a source component of continental and oceanic alkaline magmas to account for their trace-element and isotopic characteristics. Alternatively, these features have been attributed to sources containing veined, metasomatized lithosphere. In melting experiments on natural amphibole-rich veins at 1.5 gigapascals, we found that partial melts of metasomatic veins can reproduce key major- and trace-element features of oceanic and continental alkaline magmas. Moreover, experiments with hornblendite plus lherzolite showed that reaction of melts of amphibole-rich veins with surrounding lherzolite can explain observed compositional trends from nephelinites to alkali olivine basalts. We conclude that melting of metasomatized lithosphere is a viable alternative to models of alkaline basalt formation by melting of recycled oceanic crust with or without sediment.

Trace-element and isotopic characteristics of alkaline [i.e., nepheline (ne)–normative] basalts from ocean islands and continents suggest the presence of enriched components in their mantle sources (*1*). These components are often interpreted as derived from recycled oceanic crust with or without sediment (*1*). An alternative is that the enriched components are recycled, metasomatized lithospheric mantle (*2*–*6*). Although both hypotheses are compatible with trace-element and isotopic characteristics of oceanic and continental alkaline magmas, they must also be capable of accounting for the distinctive major- and minor-element characteristics of alkaline basalts (Fig. 1).

Although basic to ultrabasic ne-normative liquids can be produced by low-degree melting of garnet lherzolite, no high-pressure melting experiments on "dry" peridotite have produced melt compositions that are plausible parents of alkaline ocean-island basalts (OIBs) (*7*–*10*). Addition of CO_2 to peridotite substantially modifies liquid compositions: Near-solidus melts are carbonatitic (*11*, *12*), but with increasing temperature, low-degree melts are silica-poor and CaO- and CO_2-rich (*11*). Such findings suggest that ne-normative magmas similar to natural alkaline basalts could be produced by low-degree melting (2 to 5%) of primitive mantle sources

Division of Geological and Planetary Sciences, California Institute of Technology, Pasadena, CA 91125, USA.

*To whom correspondence should be addressed. E-mail: sebastien.pilet@unil.ch

containing 0.1 to 0.25 weight percent (wt %) CO_2 (*11*). However, primitive mantle is too poor in TiO_2 to produce in this way melts with the high TiO_2 contents of alkaline basalts (*13*); this is consistent with the premise of both of the above hypotheses that components in addition to normal mantle peridotite are required in the sources of these magmas.

The melting of recycled oceanic crust has been investigated experimentally, and high-pressure partial melts of quartz and coesite eclogites (approximating average oceanic crust at high pressures) are hypersthene (hy)–normative, not ne-normative (i.e., they are silica-oversaturated rather than alkaline) (*14*, *15*) and thus cannot produce alkaline magmas directly. A possible resolution is that silica-oversaturated oceanic crust transforms to silica-deficient garnet pyroxenite by the extraction of silica-rich fluids or melts during subduction (*16*, *17*). High-pressure melting experiments on silica-deficient garnet-clinopyroxenite compositions, either dry (*16*, *17*) or with CO_2 (*18*), have indeed produced ne-normative liquids close in some respects to the compositions of alkaline basalts (Fig. 1). However, liquids from such experiments do not reproduce the K_2O contents of alkaline basalts (Fig. 1G), and the expected trace-element compositions of these liquids, although not addressed in these experimental studies, are dependent on the processes assumed for the origin of the silica-deficient pyroxenite sources and are consequently poorly constrained.

Hydrous minerals and enrichments in incompatible elements in mantle xenoliths demonstrate that metasomatism occurs in lithospheric mantle (*19*). Here, we present results of melting experiments on natural hornblendite and clinopyroxene (cpx) hornblendite to investigate whether melting of metasomatic hydrous veins could produce liquids consistent with the major- and trace-element compositions of alkaline magmas.

We selected hornblendite (AG4) and cpx hornblendite (AG7) starting materials from the French Pyrenees because they contain amphiboles (amph) typical of those in hydrous veins from the oceanic and continental lithosphere (Fig. 2). We conducted piston-cylinder experiments on these compositions at 1.5 GPa (corresponding to a depth of ~45 km, i.e., within the lithospheric mantle) and 1150° to 1400°C for 24 to 64 hours (*20*).

Glass compositions from experiments on both vein compositions were strongly alkaline (normative ne + leucite > 18 wt % for AG4 and > 11 wt % for AG7), and all had ≤44.1 wt % SiO_2 (Fig. 1A). Glasses from experiments at 1250° to 1300°C for both compositions overlapped the compositional fields of nephelinites and basanites from ocean islands and continental settings for most elements (Fig. 1 and fig. S1). Compositional similarities between initial partial melts of AG4 and AG7 reflected incongruent melting of amphibole in both lithologies [amph → ~0.6 melt + 0.3 cpx + minor olivine (ol) + spinel (sp)] at ~1150°C, the solidus for both compositions; that is, the composition of the subsolidus amph rather than the abundance

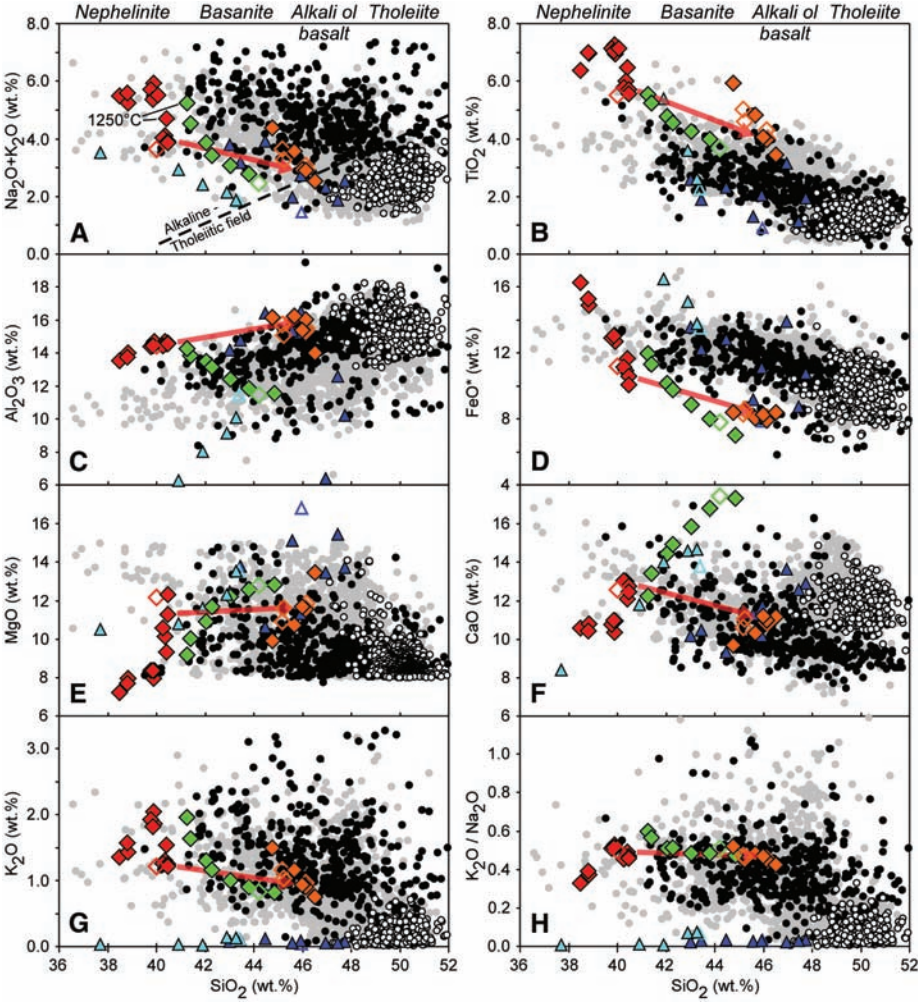

Fig. 1. Major oxides (**A** to **G**) and K_2O/Na_2O (**H**) versus SiO_2 (volatile-free) for hornblendite, clinopyroxene-hornblendite, sandwich experiments (hornblendite + peridotite), and silica-deficient garnet-pyroxenite melts (±CO_2) compared to continental and oceanic intraplate basalts and mid-ocean ridge basalt (MORB) compositions. The Macdonald-Katsura line [dashed line in (A)] separates alkaline from tholeiitic basalts. Positions of the terms nephelinite, basanite, alkali olivine (ol.) basalt, and tholeiite along the top of (A) and (B) denote the approximate silica values of each rock type. Solid gray circles, OIBs; solid black circles, continental intraplate basalts; open black circles, MORBs [all rock compositions are from GEOROC and PetDB databases (*36*) and have 8 to 15 wt % MgO]. Solid red and green diamonds, glass compositions from 1.5-GPa experiments on AG4 and AG7, respectively (the open diamonds are the starting compositions). Solid and open orange diamonds, glass compositions from 1.5-GPa sandwich experiments where orthopyroxene is present or absent, respectively, in the peridotitic layers. Solid dark and light blue triangles, glass compositions from 2- to 5-GPa experiments on silica-deficient garnet pyroxenites, dry (*16*, *17*) and in the presence of 5 wt % CO_2 (*18*), respectively (the open triangles are the starting compositions). The orange arrow in each panel connects the AG4 melt compositions to the compositions of glasses produced at same temperature (1300°C) in the sandwich experiments (AG4 + peridotite) and illustrates how melt compositions change with the assimilation of orthopyroxene (+ spinel) from the peridotite layers.

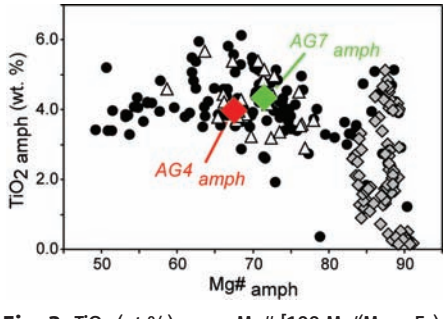

Fig. 2. TiO_2 (wt %) versus Mg# [100 Mg/(Mg + Fe), molar] for amphiboles from AG4 and AG7 (the starting materials used in this study; red and green diamonds, respectively) compared to amphiboles from oceanic and continental lithospheric veins (black circles), amphibole xenocrysts from continental basanites (open triangles), and amphiboles from metasomatized peridotite (gray diamonds) (*20*).

of cpx in the starting material was the major control on the solidus temperature and the composition of the initial melt. However, the liquidus temperatures of the two compositions were different: AG7 (with 45 wt % cpx) had a higher liquidus temperature than AG4 (with no observed cpx), ~1385°C versus ~1315°C.

The trace-element patterns of AG4 and AG7 experimental glasses were similar to those of the starting materials (Fig. 3A) but were progressively enriched relative to them with decreasing melt fraction and were somewhat enriched in more-incompatible relative to less-incompatible elements. The patterns of the starting materials and their partial melts were also generally similar to those of alkaline lavas, including features such as positive Nb and negative Pb anomalies (*1*) and elevated La/Yb ratios. In summary, the melts of amphibole-bearing metasomatic veins at 1.5 GPa were similar in major-, minor-, and trace-element compositions to those of oceanic and continental nephelinites and basanites.

The compositional continuum from nephelinites to alkali olivine basalts shown in Fig. 1 is observed in many alkaline suites (*21*, *22*). The trace-element patterns are generally similar for the various basic magmas from a single province, but with overall trace-element concentrations decreasing with decreasing alkalinity (i.e., as magmas become less ne-normative) (Fig. 3, C and D). This decrease in trace-element concentrations has been used to suggest that the continuum from nephelinite to alkali olivine basalt reflects an increase in the degree of partial melting of a common source (*21*, *22*); however, this continuum could also be explained by mixing of alkaline and tholeiitic liquids or reaction between nephelinitic or basanitic liquid and surrounding peridotite (*23*).

To test this latter hypothesis, we performed sandwich experiments in which a layer of AG4 hornblendite was packed between layers of moderately depleted peridotite (DMM1) (*24*) at 1.5 GPa and 1225° to 1325°C. The sandwich experiments yielded reactions between partial melts of the hornblendite (i.e., nephelinitic melts) and peridotite, even though temperatures were below the estimated anhydrous DMM1 solidus [~1330°C (*24*, *25*)]. Glasses from these experiments (Fig. 1) had SiO_2 contents 5 to 6 wt % higher than glasses from AG4 experiments at similar conditions (and therefore had lower normative nepheline; i.e., from ~4.5 wt % ne to ~2.0 wt % hy); somewhat lower TiO_2, FeO*, CaO, Na_2O, K_2O, and H_2O contents; and higher Al_2O_3 and MgO contents. Glasses from the sandwich experiments were generally similar to oceanic and continental alkaline basalts with 44 to 47 wt % silica (Fig. 1), and trends extending from the glasses from the hornblendite-only experiments to those from the sandwich experiments (red arrows in Fig. 1) paralleled the well-defined natural trends from nephelinites and basanites to alkali olivine basalts. The trace-element patterns of the sandwich experiments were parallel to, but ~25% lower than, those in glasses from AG4 experiments at the same temperature (Fig. 3B). These results suggest that major- and trace-element trends from nephelinites and basanites to alkali olivine basalts and tholeiites could be explained by interaction between hydrous nephelinitic melt and spinel peridotite dominated by reaction between the low-silica melt and orthopyroxene, generating a higher-silica melt plus olivine.

Two scenarios have been proposed for the production of alkaline magmas by melting of metasomatized lithosphere: (i) Shortly after or coincident with metasomatism, the lithosphere experiences a thermal perturbation or decompression and thereby melts in situ without recycling through the deeper mantle (*3*, *5*, *19*, *26*); or (ii) the metasomatized lithosphere is recycled into the convecting mantle by subduction or delamination and melts during later upwelling (e.g., in a plume) (*2*–*6*). The presence in continental alkaline magmas (*27*) of amphibole xenocrysts compositionally similar to amphiboles in metasomatic veins (Fig. 2 and fig. S2) and in metasomatized peridotite xenoliths (*19*) is consistent with the in situ hypothesis; that is, these xenocrysts and xenoliths could come from veins and associated cryptically metasomatized lithosphere formed during an earlier stage of volcanic activity that subsequently melted to produce the host alkaline magmas (*19*, *26*). The time between metasomatism of the lithosphere and the formation of the alkaline magmas cannot exceed the age of the lithosphere; however, long times are required to explain the range of isotopic ratios observed in some OIBs (e.g., from Tahaa, Rarotonga, Tubuai, etc., in Polynesia) (*3*, *6*). The recycling scenario (*2*–*6*) could account for these long time scales: Such recycling could isolate metasomatic veins for times sufficient (1 billion to 2 billion years) for ingrowth of extreme isotopic ratios such as those observed in the OIBs from Polynesia (*6*).

Note that the details of melting of recycled metasomatic veins are likely to differ from those of our experiments; because amphiboles in lithospheric veins are not stable above 2.5 to 3 GPa (~100 km depth), deep recycling of these veins would result in amphibole breakdown, and thus subsequent melting of the veins during upwelling would involve dehydrated equivalents of the hydrous compositions we have studied. Experiments on dehydrated AG4 at 1.5 GPa (*20*) (table S1) show that glass compositions are still strongly ne-normative [consistent with experiments on

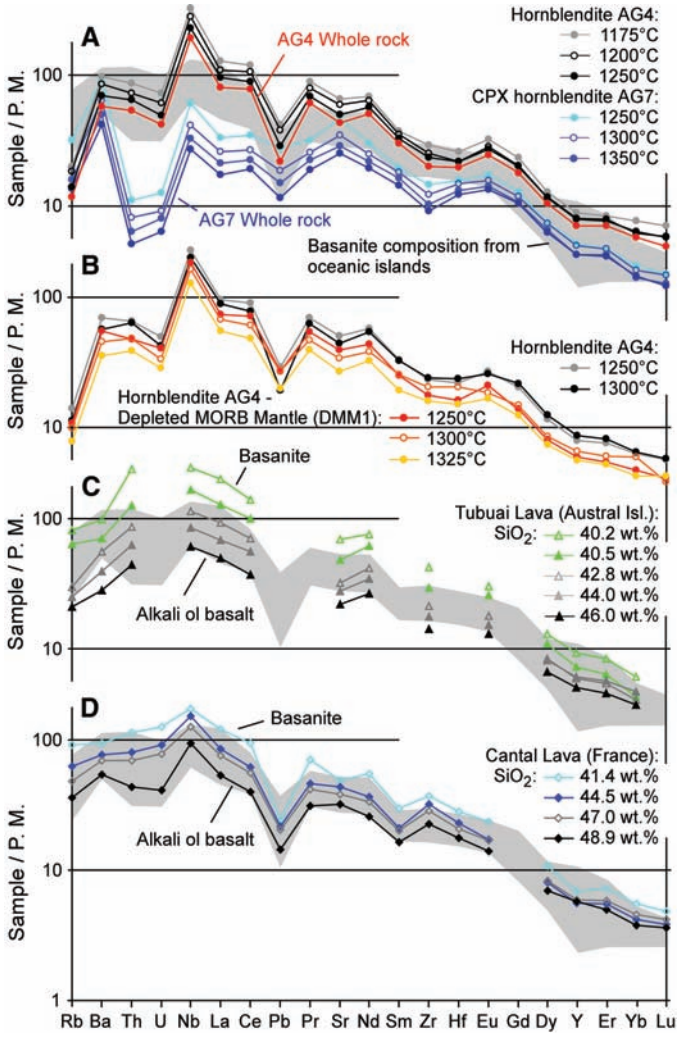

Fig. 3. Primitive mantle (*2*)–normalized trace-element abundances for (**A**) hornblendite and clinopyroxene-hornblendite melts, (**B**) melts produced in the hornblendite (AG4) + peridotite sandwich experiments (results from the 1250° and 1300°C AG4 melting experiments are shown for comparison), and (**C** and **D**) basanites (SiO_2 < 45 wt %) to alkali olivine basalts (SiO_2 > 45 wt %) from the island of Tubuai (Polynesia islands) (*22*) and the Cantal massif (France) (*6*). The gray band in (A), (C), and (D) shows the range (defined as ±1σ of the average of 195 analyses) of trace-element contents in low-silica OIB lavas (40 to 44 wt % SiO_2) with 8 to 15 wt % MgO [compiled from the GEOROC database (*36*)].

silica-poor garnet pyroxenites (*16*, *17*)] and similar to those produced in the experiments on the hydrated AG4 composition, which suggests that even deeply recycled metasomatized lithosphere could produce nephelinitic and basanitic magmas.

Although our data are consistent with the hypothesis that alkaline magmas are produced by melting of metasomatic veins, they do not provide constraints on vein formation mechanisms. The most widely cited mechanism is that these veins crystallize from low-degree melts of H_2O- and CO_2-bearing garnet peridotite (*4*, *5*, *28*, *29*), but individual veins are not thought to be representative of these low-degree melts (fig. S3). Instead, veins are explained as concentrations of phases crystallized from such melts as they cooled on ascent through the lithosphere, generating a continuum from anhydrous to hydrous assemblages (plus cryptically metasomatized adjacent peridotite) (*28*, *29*), and it is these fractionated cumulate assemblages that are the hypothesized sources of nephelinitic and basanitic magmas. Partial melts of amphibole-bearing veins formed as cumulates from low-degree mantle melts would have features characteristic of the trace-element patterns of alkaline lavas (*20*). For example, the positive Nb/La and Ce/Pb ratios observed in metasomatic veins (Fig. 3A and fig. S4) and in basic alkaline magmas (*1*) would not be interpreted as a characteristic of the mantle sources of the metasomatic liquid but would instead reflect amphibole-liquid distribution coefficients [$D_{Nb}^{amph/liq} > D_{La}^{amph/liq}$ and $D_{Ce}^{amph/liq} > D_{Pb}^{amph/liq}$ (*30*, *31*)]. On the other hand, some compositional characteristics of the metasomatic veins would be inherited directly from the low-degree melts of garnet peridotite from which they crystallize—for example, the high La/Yb ratios observed in whole-vein compositions (Fig. 3A) and in amphibole separates (fig. S4).

An important element of any model for the petrogenesis of alkaline basalts that invokes the melting of lithospheric lithologies (e.g., oceanic crust, with or without sediment or metasomatic veins) during upwelling is that the solidi of these lithologies must be lower than that of the enclosing peridotite. This point is satisfied by amphibole-bearing veins (or their dehydrated equivalents) and by oceanic crust [as eclogite (*15*) or after transformation into silica-deficient garnet pyroxenite (*16*, *17*)]. However, an aspect of decompression melting of a multilithologic mantle is that the various lithologies each influence the other's melting behavior, such that knowledge of the melting behaviors of the individual lithologies is not necessarily a guide to their behavior when they ascend together in a parcel of upwelling mantle (*32*, *33*). For example, suppose low-solidus vein material embedded in high-solidus peridotite begins to melt during adiabatic decompression but maintains thermal equilibrium with the adjacent, unmelted peridotite. In such a case, the degree of melting of the veins will be enhanced relative to the amount of melting that the same vein material would undergo if it were not embedded in the peridotite; meanwhile, the required latent heat essentially refrigerates the enclosing peridotite, and thus it will melt at lower pressure and to lower degrees than if the veins were not present (*33*). Thus, it can be anticipated that low-solidus vein material in upwelling mantle would melt more, relative to expectations based on its initial potential temperature, and that the peridotite would melt less (*32*, *33*). Therefore, recycled lithologies characterized by low solidus temperatures that are embedded in peridotite will likely melt to moderate to high degrees (especially if the enclosing peridotite also exceeds its solidus at some point during the ascent). However, subducted oceanic crust would have to melt to a low extent (≤1%) in order to explain the high trace-element contents of alkaline OIBs (*34*); such low degrees of melting seem inconsistent with the analysis above, and thus it is difficult to envision oceanic crust [or silica-deficient pyroxenite residual to extraction of fluids or melts from subducted oceanic crust (*16*, *17*)] as major trace element–bearing components of the sources of alkaline basalts. In sum, the consequences of multilithologic decompression melting are consistent with our experimental results, which suggest that high degrees of melting of metasomatic veins best explain the major- and trace-element contents of alkaline basalts.

Our results imply that the enriched component in alkaline basalts should not necessarily be equated with recycled oceanic crust and suggest that recycled components in the sources of islands characterized by tholeiitic magmas (i.e., Hawaii or Iceland) interpreted as recycled oceanic crust (*35*) are distinct from those in the sources of islands where ne-normative compositions are dominant (i.e., Polynesia, islands in the Atlantic Ocean, etc.). They also suggest that alkaline magmas are produced by high degrees of melting of a volumetrically minor mantle component rather than low degrees of melting of the dominant peridotite component. If so, these alkaline rocks do not carry as much information about the major components of the convecting mantle as is often presumed. Finally, the ranges in isotopic ratios observed in alkaline lavas from a single oceanic island do not necessarily imply the interaction between distinct mantle components such as high μ ($\mu = {}^{238}U/{}^{204}Pb$), enriched mantle, and depleted MORB mantle (*1*). Instead, they could reflect in part the time-integrated history of a suite of veins with variable trace-element ratios (e.g., Nb/Th, Ba/Nb, and Ce/Pb; including ratios that control the evolution of critical isotopic systems such as U/Pb, Rb/Sr, and Sm/Nd) (*6*) resulting from percolative fractional crystallization of metasomatic agents in the lithosphere (*6*, *28*).

References and Notes

1. A. W. Hofmann, *Nature* **385**, 219 (1997).
2. S. S. Sun, W. F. McDonough, in *Magmatism in the Ocean Basins*, A. D. Saunders, M. J. Norry, Eds., Geological Society Special Publication 42 (Blackwell Scientific, Oxford, 1989), pp. 313–345.
3. A. N. Halliday *et al.*, *Earth Planet. Sci. Lett.* **133**, 379 (1995).
4. Y. L. Niu, M. J. O'Hara, *J. Geophys. Res.* **108**, 10.1029/2002JB002048 (2003).
5. D. McKenzie, R. K. O'Nions, *J. Petrol.* **36**, 133 (1995).
6. S. Pilet, J. Hernandez, P. Sylvester, M. Poujol, *Earth Planet. Sci. Lett.* **236**, 148 (2005).
7. E. Takahashi, I. Kushiro, *Am. Mineral.* **68**, 859 (1983).
8. K. Hirose, I. Kushiro, *Earth Planet. Sci. Lett.* **114**, 477 (1993).
9. I. Kushiro, in *Earth Processes: Reading the Isotopic Code*. A. Basu, S. Hart, Eds. (American Geophysical Union, Washington, DC, 1996), pp. 109–122.
10. M. J. Walter, *J. Petrol.* **39**, 29 (1998).
11. R. Dasgupta, M. M. Hirschmann, *J. Petrol.* **48**, 2093 (2007).
12. K. Hirose, *Geophys. Res. Lett.* **24**, 2837 (1997).
13. J. Prytulak, T. Elliott, *Earth Planet. Sci. Lett.* **263**, 388 (2007).
14. T. H. Green, D. H. Green, A. E. Ringwood, *Earth Planet. Sci. Lett.* **2**, 41 (1967).
15. M. Pertermann, M. M. Hirschmann, *J. Petrol.* **44**, 2173 (2003).
16. M. M. Hirschmann, T. Kogiso, M. B. Baker, E. M. Stolper, *Geology* **31**, 481 (2003).
17. T. Kogiso, M. M. Hirschmann, D. J. Frost, *Earth Planet. Sci. Lett.* **216**, 603 (2003).
18. R. Dasgupta, M. M. Hirschmann, K. Stalker, *J. Petrol.* **47**, 647 (2006).
19. F. E. Lloyd, D. K. Bailey, *Phys. Chem. Earth* **9**, 389 (1975).
20. See supporting material on *Science* Online.
21. F. A. Frey, D. H. Green, S. D. Roy, *J. Petrol.* **19**, 463 (1978).
22. M. Caroff, R. C. Maury, G. Guille, J. Cotten, *Contrib. Mineral. Petrol.* **127**, 369 (1997).
23. C. C. Lundstrom, J. Gill, Q. Williams, *Chem. Geol.* **162**, 105 (2000).
24. L. E. Wasylenki, M. B. Baker, A. J. R. Kent, E. M. Stolper, *J. Petrol.* **44**, 1163 (2003).
25. M. M. Hirschmann, *Geochem. Geophys. Geosyst.* **1**, 10.1029/2000GC000070 (2000).
26. S. Pilet, J. Hernandez, F. Bussy, P. J. Sylvester, *Geology* **32**, 113 (2004).
27. J. B. Dawson, J. V. Smith, *Mineral. Mag.* **45**, 35 (1982).
28. B. Harte, R. H. Hunter, P. D. Kinny, *Philos. Trans. R. Soc. London Ser. A* **342**, 1 (1993).
29. E. M. Morris, J. D. Pasteris, *Mantle Metasomatism and Alkaline Magmatism*, Special Paper 215 (Geological Society of America, Boulder, CO, 1987).
30. M. Tiepolo *et al.*, *Geochem. Geophys. Geosyst.* **1**, 10.1029/2000GC000064 (2000).
31. M. Tiepolo *et al.*, *Earth Planet. Sci. Lett.* **176**, 185 (2000).
32. M. M. Hirschmann, E. M. Stolper, *Contrib. Mineral. Petrol.* **124**, 185 (1996).
33. E. M. Stolper, P. D. Asimow, *Am. J. Sci.* **307**, 1051 (2007).
34. A. Stracke, M. Bizimis, V. J. M. Salters, *Geochem. Geophys. Geosyst.* **3**, 10.1029/2001GC000223 (2003).
35. A. V. Sobolev *et al.*, *Science* **316**, 412 (2007); published online 28 March 2007 (10.1126/science.1138113).
36. GEOROC database (http://georoc.mpch-mainz.gwdg.de/georoc); PetDB database (www.petdb.org/petdbWeb/index.jsp).

37. We thank S. Newman and A. Ulianov for their help during data acquisition by Fourier transform infrared spectroscopy and laser ablation inductively coupled plasma mass spectrometry, respectively, and B. Azambre and J. Hernandez for their help during sample collection. Supported by the Swiss National Science Foundation, the Société Académique Vaudoise, and NSF grant EAR-9528594.

Supporting Online Material

www.sciencemag.org/cgi/content/full/320/5878/916/DC1
Materials and Methods
Figs. S1 to S4
Tables S1 to S3
References

15 February 2008; accepted 2 April 2008
10.1126/science.1156563